

A division in PIN-mediated patterning during lateral organ initiation in grasses: Computational model description

Devin L. O'Connor Adam Runions Aaron Sluis Jennifer Bragg John P. Vogel
 Przemyslaw Prusinkiewicz Sarah Hake

1 Introduction

The objective of the computational model is to verify whether the conceptual model of auxin transport and polarization of PIN1a, PIN1b and SoPIN1 proteins postulated in the paper can plausibly capture the experimentally observed spatio-temporal pattern of convergence point emergence, vascular strand initiation, and regions of expression and polarities of the three PINs in *Brachypodium*. The computational model was implemented in C++ using the VVE system (an extension of the Vertex-Vertex (VV) system [1]), which provides a data-structure and libraries for representing cellular tissues.

A longitudinal section of the apex is modeled as a regular 2D array of hexagonal cells. Each cell stores the concentration of auxin and the distribution of PIN1a, PIN1b and SoPIN (Fig. M1, left). For simplicity, intercellular space is not modeled, reflecting the assumption that auxin accumulation and diffusion along cell walls in the intercellular space are relatively small and can be neglected (*c.f.* [2,3]). Furthermore, cells are assumed to have unit volume, and cell walls are assumed to have unit length (*c.f.* [2,3]).

2 Auxin transport

The change of auxin concentration c_i in cell i is captured by the following equation [2,3]:

$$\frac{dc_i}{dt} = H_i - \mu c_i - \sum_j \Phi_{ij}. \quad (1)$$

Parameter H_i characterizes the rate of auxin biosynthesis in cell i (all parameter values are provided in Tables S2 and S3). Auxin turnover in the cell is modeled by the term μc_i , where μ is the rate of turnover. The final term $\sum_j \Phi_{ij}$ represents auxin transport between cell i

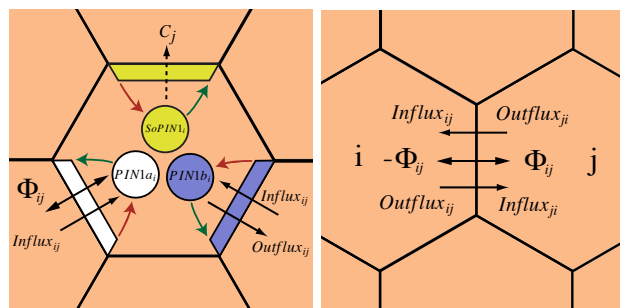


Figure M1: Diagrams explaining basic properties of the proposed model of polar auxin transport. Left: schematic view of a cell and its neighbours that illustrates the factors determining PIN allocation to segments of the cell membrane. PIN1a is shown in white, PIN1b in blue and SoPIN1 in yellow. Unallocated PINs in the cell (colored circles) are moved to the cell membrane by exocytosis (green arrows) and removed from the membrane by endocytosis (red arrows). Black solid and dashed arrows show the factors determining the allocation of each PIN protein. Solid arrows correspond to fluxes through cell faces (see right panel), which contribute to the endocytosis and exocytosis of PIN1a and PIN1b. For PIN1a, exocytosis is increased by *total* auxin flux through the membrane, and endocytosis is increased by influx through the membrane. For PIN1b, exocytosis is increased by auxin *outflux* through the membrane, and endocytosis is increased by influx. For SoPIN1, allocation to the membrane is increased by high auxin concentration in the neighbouring cell (c_j), as indicated by the dashed arrow. Right: directions of net flux, influx and outflux through the face separating cell i from cell j .

and its neighbouring cells. A net flux Φ_{ij} is the difference between $\text{Outflux}_{ij} \geq 0$, the outflux of auxin from cell i to j , and $\text{Influx}_{ij} \geq 0$, the influx of auxin from cell j to i (Fig. M1, right):

$$\Phi_{ij} = \text{Outflux}_{ij} - \text{Influx}_{ij}. \quad (2)$$

The outflux is captured by the equation

$$\begin{aligned} Outflux_{ij} = & T_{PIN1a}[PIN1a_{ij}]c_i \\ & + T_{PIN1b}[PIN1b_{ij}]c_i \\ & + T_{SoPIN1}[SoPIN1_{ij}]c_i \\ & + Tc_i. \end{aligned} \quad (3)$$

The first three terms represent outflux due to active auxin transport by PIN1a, PIN1b and SoPIN1, respectively. The last term represents basal outflux, which can be attributed to residual amounts of any efflux carrier. In the first term, the transport rate T_{PIN1a} captures the efficiency of PIN1a-dependent transport, and $[PIN1a_{ij}]$ is the concentration of PIN1a on the membrane of cell i facing cell j . The second and third terms have a similar form, but refer to the transport rates and membrane concentrations of PIN1b and SoPIN1, respectively. In the last term, T is a coefficient capturing the efficiency of basal transport.

Auxin accumulation and diffusion in the intracellular space is ignored. Consequently, $Influx_{ij} = Outflux_{ji}$: the influx of auxin into cell i from cell j ($Influx_{ij}$) is equal to the outflux of auxin from cell j towards cell i ($Outflux_{ji}$). The form of the equations capturing auxin influx and outflux is thus the same, except that outflux depends on the cell itself, whereas influx depends on its neighbors. Taken together, Equations 1–3 are consistent with those used in previous simulations of polar auxin transport [2, 4–6], but take into consideration three different PIN1s rather than one.

3 PIN polarization

The three PINs are independently produced in each cell and allocated to the cells membranes. Their localization patterns exhibit significant spatio-temporal differences (Figs. 2 and 3 in the main text), indicating a functional division between PIN1a, PIN1b and SoPIN1 in *Brachypodium*.

3.1 PIN1a and PIN1b

PIN1a and PIN1b proteins are allocated to the cell membrane from a pool of unallocated PINs that reside in the cell’s endoplasmic reticulum (ER). Their concentrations in the ER of cell i are denoted $[PIN1a_i]$ and $[PIN1b_i]$, respectively. The reported experimental data (Figs. 2 and 3) reveal allocation patterns for PIN1a and PIN1b consistent with auxin canalization. Consequently, we assume that the allocation of PIN1a and PIN1b is controlled by auxin flux [4, 5, 7].

PIN1b is expressed in large regions and polarizes towards auxin sinks (e.g., previously patterned veins). We assume that this expression is the result of outflux-based allocation and influx-based deallocation (similar to the weak polarization in [7]):

$$\begin{aligned} \frac{d[PIN1b_{ij}]}{dt} = & \sigma_{1b}[PIN1b_i] \\ & + \alpha_{1b}Outflux_{ij}[PIN1b_i] \\ & - \beta_{1b}Influx_{ij}[PIN1b_{ij}] \\ & - \nu_{1b}[PIN1b_{ij}]. \end{aligned} \quad (4)$$

The concentration of PIN1b on the membrane facing cell j thus changes as a combined result of exocytosis (terms 1 and 2) and endocytosis (terms 3 and 4). We additionally assume that this concentration cannot exceed $PIN1b_{max}$, the maximum concentration of PIN1b on a membrane (Table S2). Exocytosis consists of basal allocation (determined by basal allocation rate σ_{1b}) and allocation proportional to the outflux of auxin through the membrane (controlled by the outflux allocation rate α_{1b}). Analogously, endocytosis combines basal deallocation ν_{1b} with that proportional to auxin influx, controlled by rate coefficient β_{1b} . The assumption of linear allocation / deallocation of PIN1b results in its broad expression, which provides an effective mechanism for polarizing a tissue towards auxin sinks [5, 7].

The broad expression of PIN1b, connecting sources and sinks of auxin, is refined to a single high flux strand by PIN1a. In contrast to PIN1b, the localization of PIN1a is assumed to be non-linearly dependent on auxin flux [4, 5]:

$$\begin{aligned} \frac{d[PIN1a_{ij}]}{dt} = & \sigma_{1a}[PIN1a_i] \\ & + \gamma_{1a} \frac{(\Phi_{ij}^+)^2}{1.0 + \kappa_{1a}(\Phi_{ij}^+)^2} [PIN1a_i] \\ & - \beta_{1a} \frac{Influx_{ij}}{1.0 + \kappa_{IAA1a}c_i + \kappa_{\Phi}(\Phi_{ij}^+)^2} [PIN1a_{ij}] \\ & - \nu_{1a}[PIN1a_{ij}]. \end{aligned} \quad (5)$$

As with PIN1b, this equation captures changes of the concentration of PIN1a on the membrane facing cell j as a result of exocytosis (terms 1 and 2) and endocytosis (terms 3 and 4). Again, we clamp this value to a maximum concentration, in this case denoted $PIN1a_{max}$ (Table S2). Exocytosis consists of a basal allocation (term 1) with rate σ_{1a} and a flux-based allocation (term 2) with rate γ_{1a} . Flux-based allocation is a quadratic Hill function of positive net flux through the membrane Φ_{ij}^+ , which saturates at a rate of κ_{1a} . The quadratic dependence on flux permits a single high flux strand to emerge via an autocatalytic feedback of flux on itself [4, 5, 8, 9], as posited by the canalization hypothesis [10, 11]. Endocytosis consists of a basal deallocation (term 4) with rate ν_{1a} , and an influx-based deallocation (term 3) with the maximum rate β_{1a} . The deallocation rate decreases when auxin concentration or flux increase, as characterized by coefficients κ_{IAA1a} and κ_{Φ} , respectively. This is consistent with observations that endocytosis decreases as DR5 expression increases [12]. The linear deallocation as a function of influx restricts PIN1a localization to membranes with high auxin flux, in which quadratic term 2 dominates. This permits a functional division

between PIN1b, which controls auxin transport when flux is low, and PIN1a, which controls transport when flux is high.

Note that Equations 4 and 5 are specialized versions of a more general equation

$$\begin{aligned} \frac{d[PIN1_{ij}]}{dt} &= \sigma[PIN1_i] \\ &+ \gamma \frac{(\Phi_{ij}^+)^2}{1.0 + \kappa(\Phi_{ij}^+)^2} [PIN1_i] \\ &+ \alpha Outflux_{ij} [PIN1_i] \\ &- \beta \frac{Influx_{ij}}{1.0 + \kappa_{IAA}c_i + \kappa_\Phi(\Phi_{ij}^+)^2} [PIN1_{ij}] \\ &- \nu [PIN1_{ij}], \end{aligned} \quad (6)$$

with parameters γ , κ_{IAA} , and κ_Φ set to 0 in the case of Equation 4, and parameter β set to 0 in the case of Equation 5. The difference between polarization models of PIN1b and PIN1a can thus be viewed as quantitative rather than qualitative in nature. In particular, this difference is the result of reduced linear outflux sensing by PIN1a, compared to reduced net flux sensing by PIN1b.

Allocation of PIN1a and PIN1b to the cell membrane depends on the concentration of each in the ER of the cell. The equation for changes in the concentration of PIN1b in the ER of cell i is:

$$\begin{aligned} \frac{d[PIN1b_i]}{dt} &= \frac{\rho_{1b} + \rho_{IAA1b}c_i}{1 + \kappa_{PIN1b}[PIN1b_i]} - \mu_{1b}[PIN1b_i] \\ &- \sum_j \frac{d[PIN1b_{ij}]}{dt}. \end{aligned} \quad (7)$$

The PIN1b concentration $[PIN1b_i]$ thus changes as a combined result of production (term 1), turnover (term 2) and the exocytosis and endocytosis of PIN1b (term 3). Basal production is controlled by parameter ρ_{1b} . PIN1b production is upregulated by auxin at rate ρ_{IAA1b} [8, 13]. This production saturates at a rate controlled by κ_{PIN1b} . Turnover (term 2) occurs at rate μ_{PIN1b} . The final term, $-\sum_j \frac{d[PIN1b_{ij}]}{dt}$, describes changes in cellular PIN1b concentration due to allocation and removal of PIN1b from the cell's membranes. This is accounted for by summing changes $\frac{d[PIN1b_{ij}]}{dt}$ in PIN1b concentration at the membranes facing the neighbouring cells j (Eq. 4). The equation describing cellular changes in the concentration of PIN1a ($[PIN1a_i]$) has the same form as Equation 7:

$$\begin{aligned} \frac{d[PIN1a_i]}{dt} &= \frac{\rho_{1a} + \rho_{IAA1a}c_i}{1 + \kappa_{PIN1a}[PIN1a_i]} - \mu_{1a}[PIN1a_i] \\ &- \sum_j \frac{d[PIN1a_{ij}]}{dt}. \end{aligned} \quad (8)$$

3.2 SoPIN1

In contrast to PIN1a and PIN1b, which are involved in vein formation, the polarization pattern of SoPIN1 (Figs. 2 and 3) is consistent with the formation of convergence points. Such a pattern can be attributed to

up-the-gradient PIN polarization (towards auxin maxima) [2, 6, 13]. The assumption that SoPIN1 is polarised in a different manner than PIN1a and PIN1b is consistent with the dual-polarization model [8], except that here we attribute different polarization regimes to distinct PIN proteins, rather than different modes of operation of a single protein PIN1. Following [6, 13], we assume that SoPIN1 polarization is in a quasi-steady state. Using the equation proposed by Smith et al. [13], we thus compute the concentration $[SoPIN1_{ij}]$ associated with membrane of cell i facing cell j as:

$$[SoPIN1_{ij}] = [tSoPIN1_i] \frac{B^{c_j}}{\sum_k B^{c_k}}. \quad (9)$$

This distributes the total amount of SoPIN1 in cell i between the segments of the cell membranes according to an exponential weighting of auxin concentrations in the neighbouring cells. The weighting uses a base of $B > 1$ and is normalized by the sum of the weights assigned to each cell wall segment. As with PIN1a and PIN1b, we assume that the amount of SoPIN1 allocated to a single membrane segment is capped at a maximum value ($SoPIN1_{max}$). The remaining component of equation 8 — cellular concentration of SoPIN1 — changes according to the equation

$$\frac{d[tSoPIN1_i]}{dt} = \frac{\rho_{So1} + \rho_{IAASo1}c_i}{1 + \kappa_{SoPIN1}[tSoPIN1_i]} - \mu_{So1}[tSoPIN1_i]. \quad (10)$$

The above equation is similar to those used for $[PIN1b_i]$ and $[PIN1a_i]$ (Eqs. 7 and 8), but omits the term capturing changes due to allocation and deallocation of PIN. The reason is that $[tSoPIN1_i]$ represents the total concentration of SoPIN1 in the cell as opposed to the concentrations within the ER used for PIN1a and PIN1b.

4 Tissue-level patterning

A longitudinal section of the shoot apical meristem is approximated as a regular array of hexagonal cells divided into epidermal layers L1 and L2, and subepidermal cells (Fig. M2). The initial state of the simulation is obtained by setting auxin biosynthesis to 0 and linearly increasing it to H_i over time interval t_0 (Tables S2 and S3). Growth is emulated by adding rows of cells at the top of the tissue at regular intervals t_{growth} , counting from time t_0 . In the growing cellular template we make a number of assumptions to account for additional factors influencing polar auxin transport that are specific to the shoot and shoot apical meristem. These assumptions concern: properties of specific tissue layers, the impact of tissues that are not explicitly simulated (boundary conditions), and stabilization of convergence points.

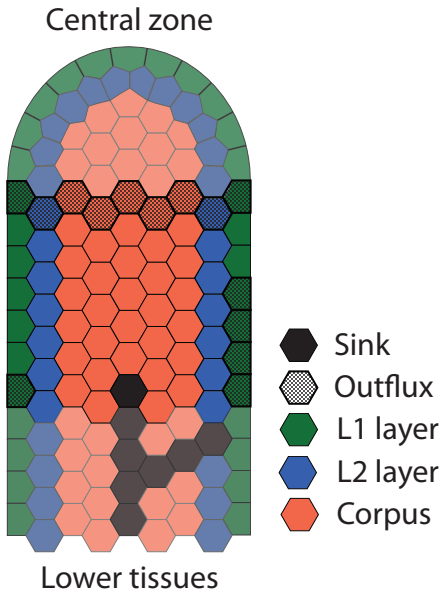


Figure M2: The layout of the cellular tissue used to simulate convergence point and vascular strand patterning. Cells in the L1 are colored green, those in the L2 blue, and corpus cells are colored red. Cells assumed to export auxin outside the explicitly modelled part of the shoot are stippled. In addition, a sink is located at the base of the tissue (black cell). Faded cells represent parts of the tissue outside the scope of the model.

4.1 Tissue layers

Previous work on tomato and *Arabidopsis* indicates that auxin response and transport are quantitatively different in the tunica and the central zone of the apex, compared to the corpus [8, 14]. The data reported for *Brachypodium* meristems in the main text are consistent with these observations. To account for these differences we make the following assumptions:

1. Auxin transport between the L1 and L2 layers is reduced compared to the remainder of the tissue. This reduction is justified by the strong gradient of auxin concentration between L1 and L2 (Figs. 2G and 3F), and represents an assumption also made in previous models [8, 13, 14]. In the present model, it is effected by reducing the efficiency of PIN transport (Eq. 3) through membranes at the interface between the L1 and L2 layers (Table S3). As in previously published models [8, 13], this reduction increases auxin accumulation in the L1, providing the auxin necessary for the formation of convergence points. Additionally, it helps insulate the L1 from sub-epidermal layers, which increases the stability of convergence point formation.
2. PIN polarization in the L1 and L2 layers favors up-the-gradient auxin transport (Figs. 2C, 2D, 3A and

3B; Video S1; see also [8]). Accordingly, in Eqs. 8-10, the expression of SoPIN1 is increased in the L1 and L2 layers, and expression of PIN1a and PIN1b is decreased (Table S3).

3. Auxin biosynthesis (Eq. 1) is increased in the L1 layer. This is supported by high DR5 expression in L1 and represents an assumption also made in previous models [8, 13, 14]. Auxin biosynthesis is controlled by setting H_i to H_{epi} in the L1 and $H_{sub} < H_{epi}$ in all other cells.

4.2 Boundary conditions

The proposed model only captures a distal portion of a shoot, excluding the central zone (Fig. M2). We make the following assumptions to simulate the effect of the shoot segment below the bottom row of cells in the model:

1. A cell representing a strong auxin sink is present at the base of the tissue. This cell removes all auxin entering it, and provides a target for the first initiating vein.
2. A pair of convergence points is present in the L1 layer of the lower tissues (with the CP on the right above that on the left). Proximal cells in the epidermis are assumed to supply auxin to these CPs at a rate of μ_{CP} (this affects the lowest cell on the left and 4 lowest cells on the right). The assumed left-right asymmetry leads to the alternate introduction of convergence points on the left and right sides of the tissue.

Finally, the rectangular layout of the tissue does not faithfully capture the geometry of the central zone. We subsume the effect of the quiescent zone on the modelled part of the SAM by removing auxin from the top row of cells at a rate of μ_{epi} in the epidermis and μ_{sub} in subepidermal cells (Table S3). Once a cell no longer occupies a position in the top row of cells (i.e. a new row is added), these rates decrease to zero over the time intervals t_{epi} (epidermis) and t_{sub} (subepidermal).

4.3 Stabilization of convergence points

Convergence points may shift their position in the L1 layer when new rows of cells are added, unless additional assumptions are introduced (c.f. [2, 8, 13]). In reality, the stabilization of auxin maxima is likely due to additional molecular compounds which are known to influence polar auxin transport, such as AUX/LAX [15, 16] and CUC2 [2] proteins. As these additional factors fall outside the scope of the current model, we approximate their effects by introducing the following assumptions concerning convergence points.

1. Epidermal cells whose auxin concentration exceeds the threshold Th_{CP} are marked as part of a convergence point, and the localization of SoPIN1 in these cells becomes fixed. This is consistent with the fixed PIN1 polarization at convergence points that results from the downregulation of CUC2 in *Arabidopsis* [2]. If auxin concentration subsequently decreases below $\frac{1}{4}Th_{CP}$, the cell will no longer be marked as part of the CP.
2. SoPIN1 polarization is biased towards cells recruited to a convergence point. As in [13], this bias is implemented by multiplying auxin concentrations c in Eq. 9 by a factor c_{CP} if the corresponding cell belongs to a CP.
3. Auxin biosynthesis increases in convergence points [13]. Once cell i becomes part of a convergence point, the rate H_i in Eq. 1 gradually increases from H_{epi} to H_{CP} over the next t_{CP} units of time in the simulation.

4.4 Parameter values

The values of all parameters used in the simulations are given in Tables S2 and S3. They are reported to assure reproducibility of our results, rather than provide the physical values. Although estimates for the values of some parameters used in our simulations exist for other species (e.g., [6, 8, 17, 18]) and could be used as approximate values for *Brachypodium distachyon*, other values, in particular those pertinent to the dynamics of auxin-driven PIN polarization, are not yet known. Consequently, following the approach of [2,3], we have chosen to use unitless parameters in our simulations (their dimensions are indicated in the last column). This is consistent with our emphasis on the qualitative nature of the interactions between SoPIN1, PIN1a and PIN1b.

The model produces convergence points and the related high-flux pre-vascular strands robustly for a wide range of parameters. With some coordination between parameters, most can be changed significantly — typically by at least one order of magnitude — while qualitatively preserving simulation results. The range of parameters is more restricted when a specific alternating pattern of convergence points is desired, as the placement of the first pair of convergence points is particularly sensitive to model parameters (which must be defined with an accuracy of $\pm 5\%$). This sensitivity is related to the assumed boundary conditions at the base of the tissue, which do not fully reproduce the presence of the pair of basal convergence points below the simulated tissue.

5 Discussion

Using a small number of assumptions differentiating the expression and polarization of SoPIN1, PIN1a and PIN1b, the model captures the patterns of their expression and polarization near the apical meristem of *Brachypodium*. In the epidermis, SoPIN1 drives the formation of convergence points. This leads to the accumulation of auxin and its outflow to the subepidermal layers. The feedback between auxin flow and PIN1b proteins polarizes them broadly towards sinks, the previously formed vascular strands. High concentration of auxin in the CP also initiates the expression of PIN1a, which increases auxin transport to sub-epidermal layers. There, canalization occurs within the region broadly specified by PIN1b, resulting in the formation of a provascular strand of highly PIN1a-polarized cells connecting the CP to a sink. Interestingly, the broad polarization of PIN1b towards the sink facilitates the finding of a sink in the present model, eliminating the use of an unidentified factor introduced in the dual polarization model [8].

References

1. Smith C, Prusinkiewicz P (2004) Simulation modeling of growing tissues. In: C Godin *et al*, editor, Proceedings of the 4th International Workshop on Functional Structural Plant Models, Montpellier: UMR AMAP. pp. 365–370.
2. Bilsborough G, Runions A, Barkoulas M, Jenkins H, Hasson A, et al. (2011) Model for the regulation of *Arabidopsis thaliana* leaf margin development. Proceedings of the National Academy of Sciences of the USA 108: 3424–3429.
3. Prusinkiewicz P, Crawford S, Smith R, Ljung K, Bennett T, et al. (2009) Control of bud activation by an auxin transport switch. Proceedings of the National Academy of Sciences of the USA 106: 17431–17436.
4. Mitchison G (1981) The polar transport of auxin and vein patterns in plants. Philosophical Transactions of the Royal Society of London B 295: 461–470.
5. Feugier F, Mochizuki A, Iwasa Y (2005) Self-organization of the vascular system in plant leaves: Inter-dependent dynamics of auxin flux and carrier proteins. Journal of Theoretical Biology 236: 366–375.
6. Jönsson H, Heisler M, Shapiro B, Meyerowitz E, Mjolsness E (2006) An auxin-driven polarized

- transport model for phyllotaxis. *Proceedings of the National Academy of Sciences of the USA* 103: 1633–1638.
7. Stoma S, Lucas M, Chopard J, Schaedel M, Traas J, et al. (2008) Flux-based transport enhancement as a plausible unifying mechanism for auxin transport in meristem development. *PLoS Computational Biology* 4: e1000207.
 8. Bayer E, Smith R, Mandel T, Nakayama N, Sauer M, et al. (2009) Integration of transport-based models for phyllotaxis and midvein formation. *Genes and Development* 23: 373–384.
 9. Rolland-Lagan AG, Prusinkiewicz P (2005) Reviewing models of auxin canalization in the context of leaf vein pattern formation in *Arabidopsis*. *The Plant Journal* 44: 854–865.
 10. Sachs T (1969) Polarity and the induction of organized vascular tissues. *Annals of Botany* 33: 263–275.
 11. Sachs T (1991) *Pattern Formation in Plant Tissues*. Cambridge: Cambridge University Press.
 12. Paciorek T, Zazimalova E, Ruthardt N, Petrasek J, Stierhof Y, et al. (2005) Auxin inhibits endocytosis and promotes its own efflux from cells. *Nature* 435: 1251–1256.
 13. Smith R, Guyomarc’h S, Mandel T, Reinhardt D, Kuhlemeier C, et al. (2006) A plausible model of phyllotaxis. *Proceedings of the National Academy of Sciences of the USA* 103: 1301–1306.
 14. Reinhardt D, Pesce E, Stieger P, Mandel T, Baltensperger K, et al. (2003) Regulation of phyllotaxis by polar auxin transport. *Nature* 426: 255–260.
 15. Heisler M, Jönsson H (2006) Modeling auxin transport and plant development. *Journal of Plant Growth Regulation* 25: 302–312.
 16. Bainbridge K, Guyomarc’h S, Bayer E, Swarup R, Bennett M, et al. (2008) Auxin influx carriers stabilize phyllotactic patterning. *Genes and Development* 22: 810–823.
 17. Grieneisen V, Xu J, Marée A, Hogeweg P, Scheres B (2007) Auxin transport is sufficient to generate a maximum and gradient guiding root growth. *Nature* 449: 1008–1013.
 18. Kramer EM (2008) Computer models of auxin transport: a review and commentary. *Journal of Experimental Botany* 59: 45–53.